Induced bronchus–associated lymphoid tissue serves as a general priming site for T cells and is maintained by dendritic cells

Stephan Halle,[1] Hélène C. Dujardin,[1] Nadja Bakocevic,[1] Henrike Fleige,[1] Heike Danzer,[1] Stefanie Willenzon,[1] Yasemin Suezer,[2] Günter Hämmerling,[3] Natalio Garbi,[3] Gerd Sutter,[4] Tim Worbs,[1] and Reinhold Förster[1]

[1]Institute of Immunology, Hannover Medical School, 30625 Hannover, Germany
[2]Paul-Ehrlich-Institute, 63225 Langen, Germany
[3]Division of Molecular Immunology, Deutsches Krebsforschungszentrum, 69120 Heidelberg, Germany
[4]Institute for Infectious Diseases and Zoonoses, University of Munich, 80539 Munich, Germany

Mucosal vaccination via the respiratory tract can elicit protective immunity in animal infection models, but the underlying mechanisms are still poorly understood. We show that a single intranasal application of the replication-deficient modified vaccinia virus Ankara, which is widely used as a recombinant vaccination vector, results in prominent induction of bronchus-associated lymphoid tissue (BALT). Although initial peribronchiolar infiltrations, characterized by the presence of dendritic cells (DCs) and few lymphocytes, can be found 4 d after virus application, organized lymphoid structures with segregated B and T cell zones are first observed at day 8. After intratracheal application, in vitro–differentiated, antigen-loaded DCs rapidly migrate into preformed BALT and efficiently activate antigen-specific T cells, as revealed by two-photon microscopy. Furthermore, the lung-specific depletion of DCs in mice that express the diphtheria toxin receptor under the control of the CD11c promoter interferes with BALT maintenance. Collectively, these data identify BALT as tertiary lymphoid structures supporting the efficient priming of T cell responses directed against unrelated airborne antigens while crucially requiring DCs for its sustained presence.

CORRESPONDENCE
Reinhold Förster:
Foerster.Reinhold@
MH-Hannover.de

Abbreviations used: AM, alveolar macrophage; BAL, bronchioalveolar lavage; BALT, bronchus-associated lymphoid tissue; brLN, bronchial LN; DT, diphtheria toxin; DTR, DT receptor; EGFP, enhanced GFP; i.n., intranasal; i.t., intratracheal; IU, infectious unit; MVA, modified vaccinia virus Ankara; SHG, second harmonics generation.

Bronchus-associated lymphoid tissue (BALT) is part of the mucosal immune system of the lung and is characterized by the aggregation of lymphoid cells at the bifurcations of the upper bronchioles (Bienenstock and Befus, 1984). Like other lymphoid follicles, BALT is composed of B cells surrounded by a parafollicular region of T cells (Sminia et al., 1989). Recirculating lymphocytes are believed to enter BALT via high endothelial venules and leave these structures by efferent lymphatics (Lührmann et al., 2002/2003; Xu et al., 2003). Although BALT is largely absent in normal mice, it spontaneously forms in mice deficient for the chemokine receptor CCR7 (Kocks et al., 2007). In humans, it is neither found at birth nor in healthy adults but transiently arises during childhood and adolescence (Tschernig and Pabst, 2000). In both humans and mice,

pulmonary infection and inflammation can induce BALT (Moyron-Quiroz et al., 2004). Data derived from splenectomized lymphotoxin-α–deficient mice, which lack all secondary lymphoid organs but do develop BALT, suggest that BALT can serve as induction sites for adaptive immune responses to pathogens with lung tropism (Moyron-Quiroz et al., 2004). However, mechanisms that control the development and maintenance of BALT are largely unknown.

Modified vaccinia virus Ankara (MVA) is a highly attenuated orthopoxvirus that lost its capacity to replicate in mammalian cells (Meyer et al., 1991). Recently, MVA was proposed to represent a useful agent for mucosal vaccination

S. Halle and H.C. Dujardin contributed equally to this paper.

via the respiratory route in a nonhuman primate model (Corbett et al., 2008). In mice, MVA delivered via the intranasal (i.n.) route has been shown to induce long-lasting and protective antibody and T cell immune responses (Gherardi and Esteban, 2005; Kastenmuller et al., 2009). However, little is known about the immunological events after respiratory MVA infection.

The present report demonstrates that a single i.n. application of the replication-deficient MVA is sufficient to induce the long-lasting presence of BALT and that the lung-specific depletion of DCs interferes with BALT maintenance. Ex vivo imaging of antigen-specific T cell–DC interactions within BALT by two-photon microscopy indicates that, independent of the specific antigenic challenge inducing its formation, BALT can function as a general priming site for T cell responses directed against antigens that reach the lower respiratory tract.

RESULTS AND DISCUSSION
A single i.n. application of replication-deficient MVA suffices to induces highly organized BALT

We have recently shown that i.n. infection with the mouse γ–herpesvirus MHV-68 induces BALT in mice and that BALT actually serves as a reservoir of latent MHV-68 (Kocks et al., 2009). To address the question of whether latent or continuous reinfection of host cells with virus is required for the induction and/or maintenance of BALT, we tested the replication-deficient poxvirus MVA for its ability to induce BALT. Although the peribronchiolar space in lungs of untreated mice contained only few CD11c$^+$ cells and hardly any lymphocytes (Fig. 1 A and not depicted), a massive perivascular and peribronchiolar infiltration of CD11c$^+$ cells could be observed 4 d after i.n. application of 10^7 infectious units (IU) MVA (Fig. 1 B). At day 8 after infection, B and T cells had been recruited to CD11c$^+$ cell–rich areas (Fig. 1, C and D). Although in some areas B and T cells were still scattered diffusely around vessels and bronchioles (Fig. 1 C) at this time point, we also frequently observed areas in which B cells started to segregate toward the center of BALT structures (Fig. 1 D). By day 12, large areas of BALT had been formed. Frequently, CD11c$^+$ cells were found surrounding the structures (Fig. 1 E), whereas B and T cells exhibited various degrees of clustering (Fig. 1 F). At day 28 after infection, the MVA–induced BALT displayed a pronounced segregation into T and B cell–rich areas (Fig. 1 G). In this differentiated BALT, DCs were found to reside primarily in the T cell areas (Fig. 1 H). Quantitative analysis revealed that BALT structures were most abundantly present between days 8 and 12 after infection but could still be detected at relatively high frequencies even 28 d after virus application (Fig. 1 I). Collectively, these data demonstrate that a single i.n. application of the replication-deficient MVA is sufficient to induce the long-lasting presence of highly organized BALT, and that the accumulation of CD11c$^+$ cells around vessels and bronchioles represents an early event in its formation.

Virus–encoded gene expression and recruitment of inflammatory cells after i.n. application of MVA

To monitor productive MVA infection and viral gene expression in the lung, we used an MVA strain encoding an enhanced GFP (EGFP; Lehmann et al., 2009). Within 5–7 h after i.n. infection, high numbers of GFP^{bright} cells could be detected in the bronchioalveolar lavage (BAL) of MVA–GFP– infected but not MVA–WT–infected animals (Fig. 2, A and B).
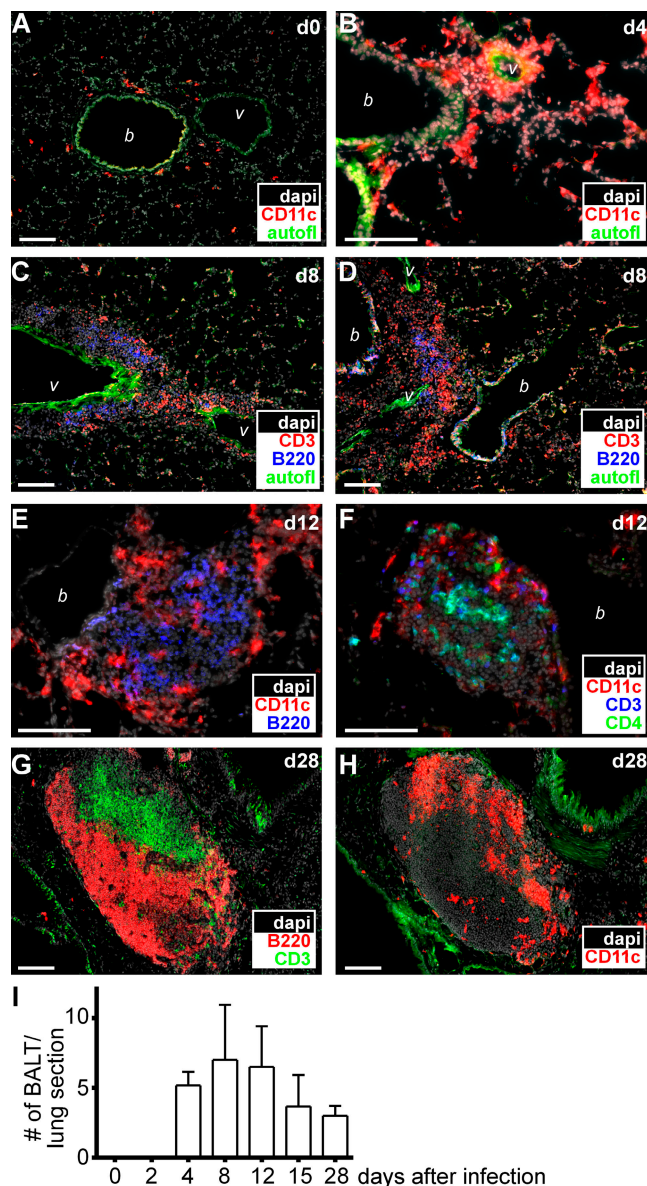

Figure 1. Induction of BALT after mucosal infection with MVA. (A–H) C57/BL6 mice were infected i.n. with 10^7 IU MVA, and at the time points indicated (days after infection), lung sections were analyzed by fluorescence microscopy applying mAb and DAPI as indicated. Representative sections from three to six mice analyzed for each time point derived from two to three different experiments are shown. Bars, 100 μm. (I) The number of BALT structures per entire central lung section was determined by microscopy (means + SD; n = 3–5 animals per time point; pooled data are derived from six independent experiments). b, bronchioles; v, vessels.

Although up to 50% of all live cells in the BAL expressed GFP at 7 h after infection, only a very small proportion of cells were still GFP[+] at 24 h after infection, and no GFP signals were detectable at later time points (Fig. 2 B). Because MVA cannot produce infectious virions in mammals (Ramírez et al., 2000), these data indicate that MVA infectivity is rapidly inactivated in vivo. Further analysis revealed that 65% of all BAL cells isolated 5–7 h after infection represented alveolar macrophages (AMs; CD11c^{+}MHCII^{−}; Fig. 2 C). More than 92% of all GFP^{+} cells showed this phenotype, with only 4% of all GFP^{+} cells being conventional DCs (CD11c^{+}MHCII^{+}; Fig. 2 D). Importantly, the analysis of single-cell suspensions prepared by enzymatic digestion of whole-lung tissue yielded largely identical results (unpublished data).

The rapid decrease of the GFP signal observed shortly after infection with MVA-GFP prevented its further use in directly tracking the fate of MVA-encoded antigenic material. To overcome this limitation, Cy5-labeled MVA

(MVA-Cy5) was subsequently used for i.n. infection. As early as 20 min after MVA-Cy5 inoculation, numerous large CD11c^{+} cells could be detected carrying MVA-Cy5 and having the typical location of AMs within the lumen of alveoli and airways (Fig. 2 E). In accordance with our data derived from i.n. MVA-GFP infection, we could also detect few Cy5^{+}CD11b^{+}CD11c^{+} DCs (Fig. 2 F) in the lungs of MVA-Cy5–infected animals. However, the CD11c^{+} DC network surrounding the conducting airway system did not harbor detectable MVA-Cy5 fluorescence (unpublished data). Analyzing BAL 3 d after infection, a significant increase in the number of DCs (CD11c^{+}MHCII^{+}; Fig. 2 G) as well as inflammatory CD11c^{−}CD11b^{hi} cells (Fig. 2 G), such as recruited monocytes/macrophages and granulocytes, could be observed. At this time point, >20% of the total BAL cells still contained MVA-Cy5 (Fig. 2 H). These MVA-Cy5^{+} cells were now exclusively CD11c^{+} and/or CD11b^{+} cells (Fig. 2 I, right), with most of them showing a phenotype of DCs
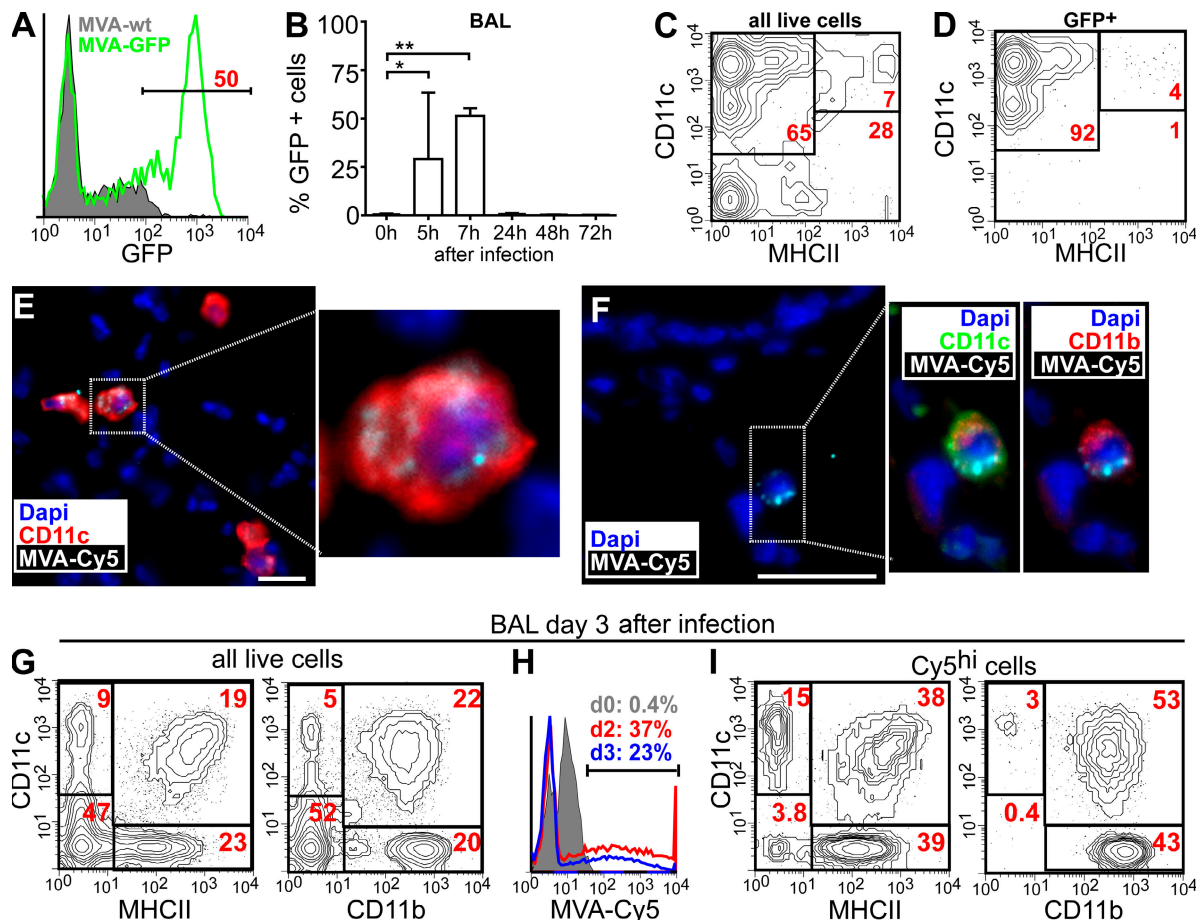

Figure 2. **Initial host cell tropism of MVA in the lung.** Mice were i.n. infected with 10[7] IU MVA, and BAL cells were analyzed by flow cytometry. (A) GFP expression of DAPI^{−} BAL cells 7 h after infection with MVA-GFP or MVA-WT. (B) GFP expression of BAL 0–72 h after i.n. infection with MVA-GFP (mean + SD; n = 2–3 mice/time point). (C and D) Expression of CD11c and MHCII on all (C) or GFP[+] (D) DAPI^{−} BAL cells 7 h after infection with MVA-GFP. (E) Immunohistology of lung sections 6 h after i.n. application of Cy5-labeled MVA using antibodies and dyes as indicated. (F) As in E, we obtained sections from lungs 30 min after MVA-Cy5 application. Bars, 25 µm. (G–I) FACS analysis of BAL cells 3 d after MVA-Cy5 application using antibodies and virus as indicated. (G and H) Gate on all DAPI^{−} cells. (I) Gate on all DAPI[−] MVA-Cy5^{+} cells. The FACS plots and immunohistology shown are representative of three independent experiments, each with two to three mice analyzed per time point. *, P < 0.05; **, P < 0.01.

(CD11c⁺MHCII⁺) or inflammatory cells (CD11b⁺CD11c⁻; Fig. 2 I, left).

Collectively, these data indicate that predominantly AMs and some DCs are efficiently infected with MVA within hours after i.n. application. Most of the infected cells rapidly disappear from the lung within a few hours, presumably undergoing apoptosis and/or necrosis, similar to processes found after in vitro infection with MVA (Liu et al., 2008). However,
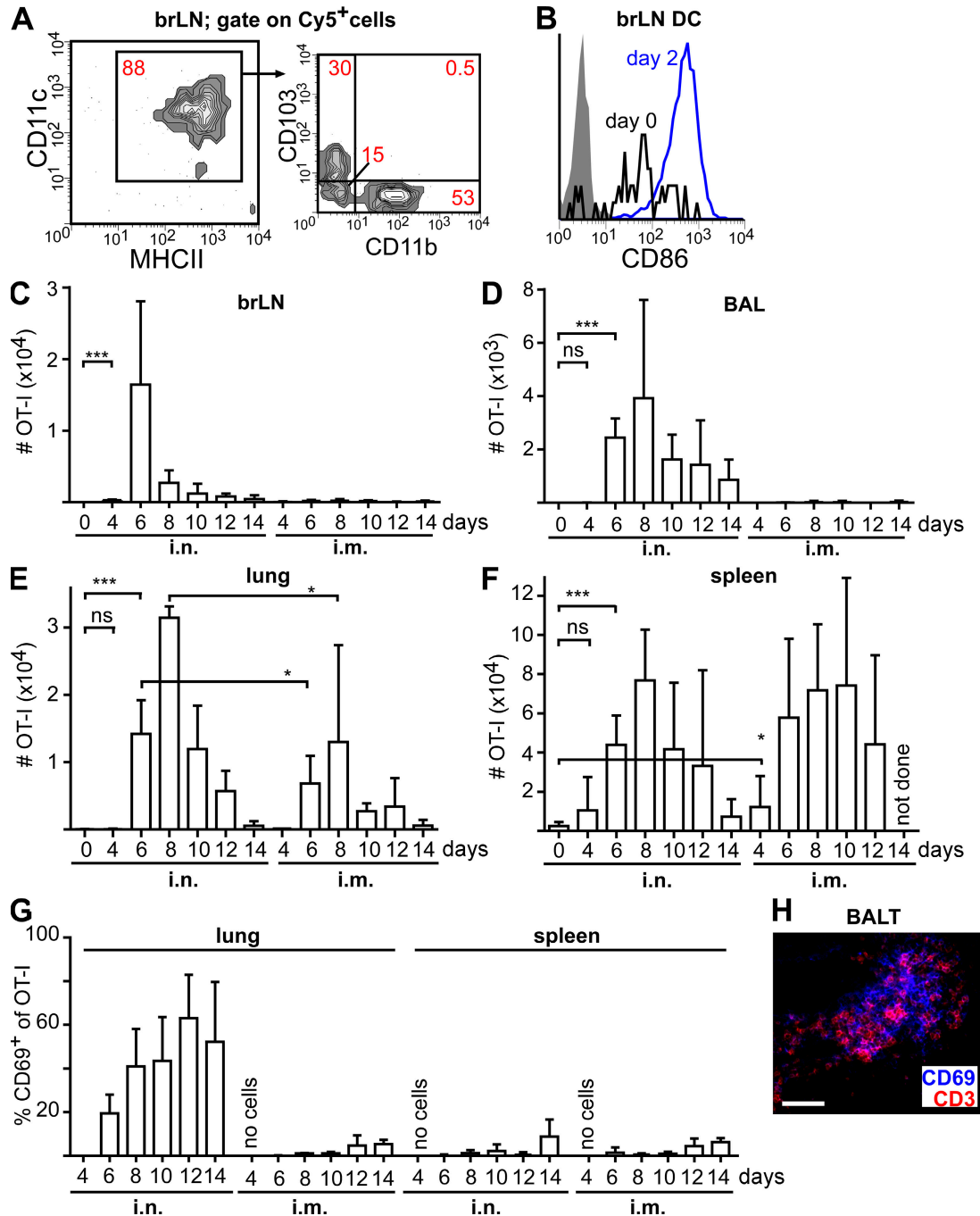

Figure 3. i.n. vaccination with recombinant MVA induces a distinct population of antigen–specific cytotoxic T cells in the lung. (A) Mice i.n. received 10^7 IU MVA-Cy5, and 3 d later the phenotype of Cy5⁺ cells in the draining LNs was determined by flow cytometry. (B) Expression of CD86 on CD11c⁺MHCII⁺ brLN DCs before and 2 d after i.n. instillation of MVA (shaded area, isotype control). (C–G) 1 d after the i.v. transfer of 200 CD45.1⁺ CD8⁺ OT-I T cells into CD45.2⁺ recipients, mice were i.n. or i.m. infected with 10^7 IU MVA-OVA. At the indicated time points (days after infection) the absolute number of OT-I cells was determined in the brLNs (C), BAL (D), lung (E), and spleen (F). (G) The percentage of OT-I cells expressing CD69 in the lung and spleen. (H) Expression of CD3 and CD69 in BALT at 12 d after infection. Bar, 50 μm. Data in A and B are representative of four mice analyzed in two independent experiments. Data shown in C–G are pooled from two independent experiments with two to three mice per time point (means + SD). *, P < 0.05; ***, P < 0.001.

at the same time, the initial MVA infection initiates a sequence of events leading to the recruitment of DCs and inflammatory cells that would also allow for the induction of adaptive immune responses.

Recombinant MVA induces a distinct population of antigen–specific cytotoxic T cells in the lung after i.n. application

After i.n. instillation of MVA-Cy5, we could readily detect Cy5^{+} cells in the lung-draining bronchial LNs (brLNs). These cells were primarily DCs expressing high levels of CD11c and MHCII (Fig. 3 A). The majority of these DCs were found to express either CD103 or CD11b (Fig. 3 A). These observations, together with the finding that brLN DCs of i.n. MVA-infected mice express higher levels of CD86 than those of noninfected mice (Fig. 3 B), indicate that the i.n. vaccination with MVA can elicit a productive immune response in the lung as well as in the lung-draining brLNs. We therefore hypothesized that the quality of an adaptive immune response directed against the model antigen OVA in the lung might differ between mucosal (i.n.) and systemic (i.m.) application of MVA encoding chicken OVA (MVA-OVA). To closely mirror the physiological situation of a small starting population of naive T cells being specific for a given antigen, we adoptively transferred by i.v. injection 200 OT–I T cells (CD45.1[+]) that recognize the SIINFEKL peptide derived from OVA in an MHC class I–restricted manner into CD45.2 recipients 1 d before infection with MVA-OVA via the i.n. or i.m. route.

After i.n. MVA-OVA application, OT–I T cells could be detected at day 4 after infection in the brLNs and spleen (Fig. 3, C and F). These cells were also found in the lung and BAL (Fig. 3, D and E) starting at day 6. In contrast, after i.m. application, only very few OT–I T cells were present in brLNs or BAL at any time point investigated (Fig. 3, C and D), whereas these cells appeared with similar kinetics and numbers in the spleen but less frequently in the lung when compared with i.n.-treated mice (Fig. 3, E and F). Of interest, after i.n. but not i.m. application, persistent expression of the early activation marker CD69 were observed on a large proportion of OT–I as well as endogenous CD8^{+} T cells in the lung and BAL (Fig. 3 G and not depicted). In contrast, hardly any expression of CD69 could be observed on OT–I T cells residing in the spleen independent of the route of MVA application (Fig. 3 G). Immunohistology of lung sections revealed that CD69^{+} T cells were present in BALT (Fig. 3 H).

These observations indicate that the application of MVA via the respiratory route can induce a local immune response that is characterized by the presence of activated antigen-specific as well as nonspecific CD8^{+} T cells in the airways (BAL) and BALT that continuously express high levels of CD69. The transient up-regulation of CD69 has recently been suggested to inhibit lymphocyte egress from LNs by retaining sphingosine 1–phosphate receptor 1, a receptor known to be required for lymphocyte exit from LNs into efferent lymphatics, within intracellular compartments (Shiow et al., 2006).

It remains to be determined whether CD69 might similarly contribute to the retention of lymphocytes within BALT or whether continuous CD69 expression represents a general feature of T cells present within the lung environment (Kohlmeier et al., 2007).

Essential role for DCs in BALT maintenance

The infiltration of CD11c^{+} DCs observed within the lungs of MVA-infected mice probably represents an early step during BALT induction (Fig. 1 B). To address the role of DCs in the maintenance of MVA-induced BALT in further detail, we i.n. applied diphtheria toxin (DT) to CD11c-DOG mice (Hochweller et al., 2008), which express the DT receptor (DTR) under the control of the CD11c promoter. The i.n. application of DT at days 8 and 10 after MVA infection resulted in an efficient depletion of CD11c^{+} cells from the lung tissue (Fig. 4 A and not depicted). A quantitative
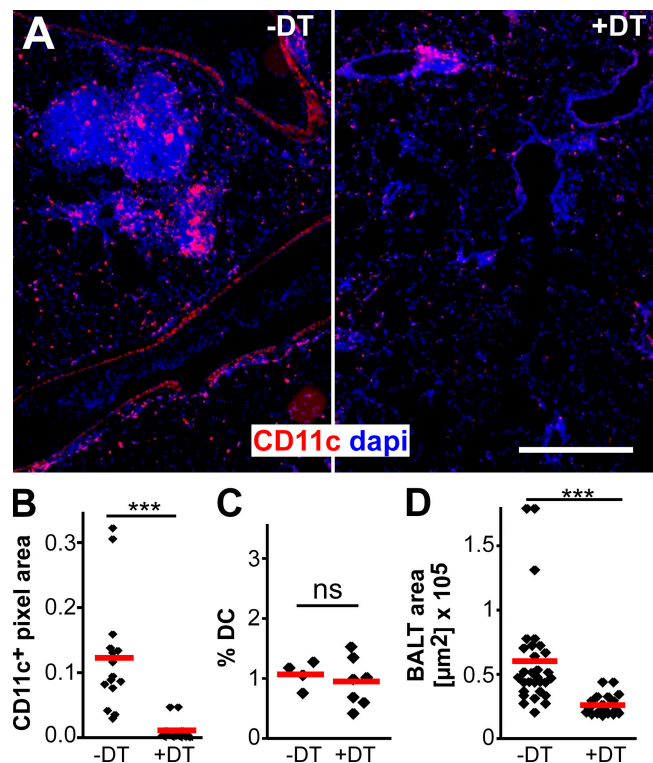

Figure 4. Local depletion of DCs interferes with BALT maintenance. Mice expressing DTR under the control of the CD11c promoter (CD11c-DOG) were infected twice with 10[7] IU MVA. On days 8 and 10, mice were treated i.n. with 50 ng DT (+DT) or with PBS (−DT). (A) Lung sections from DT-treated or untreated mice stained with DAPI and anti-CD11c. Bar, 200 µm. (B) Micrographs were quantitatively analyzed for the presence of anti-CD11c signals. (C) No change in the percentage of DCs in the mesenteric LNs was detected by flow cytometry. Pooled data from three experiments, each with one to two mice per group, are shown. (D) The number and size of individual BALT structures from DT-treated or untreated mice were determined on large composite images of entire lung sections ($n = 6$ mice /group in B and D with two to three lung sections per mouse in two independent experiments analyzed). Symbols represent the mean BALT size per lung, and red bars represent means. ***, $P < 0.001$.
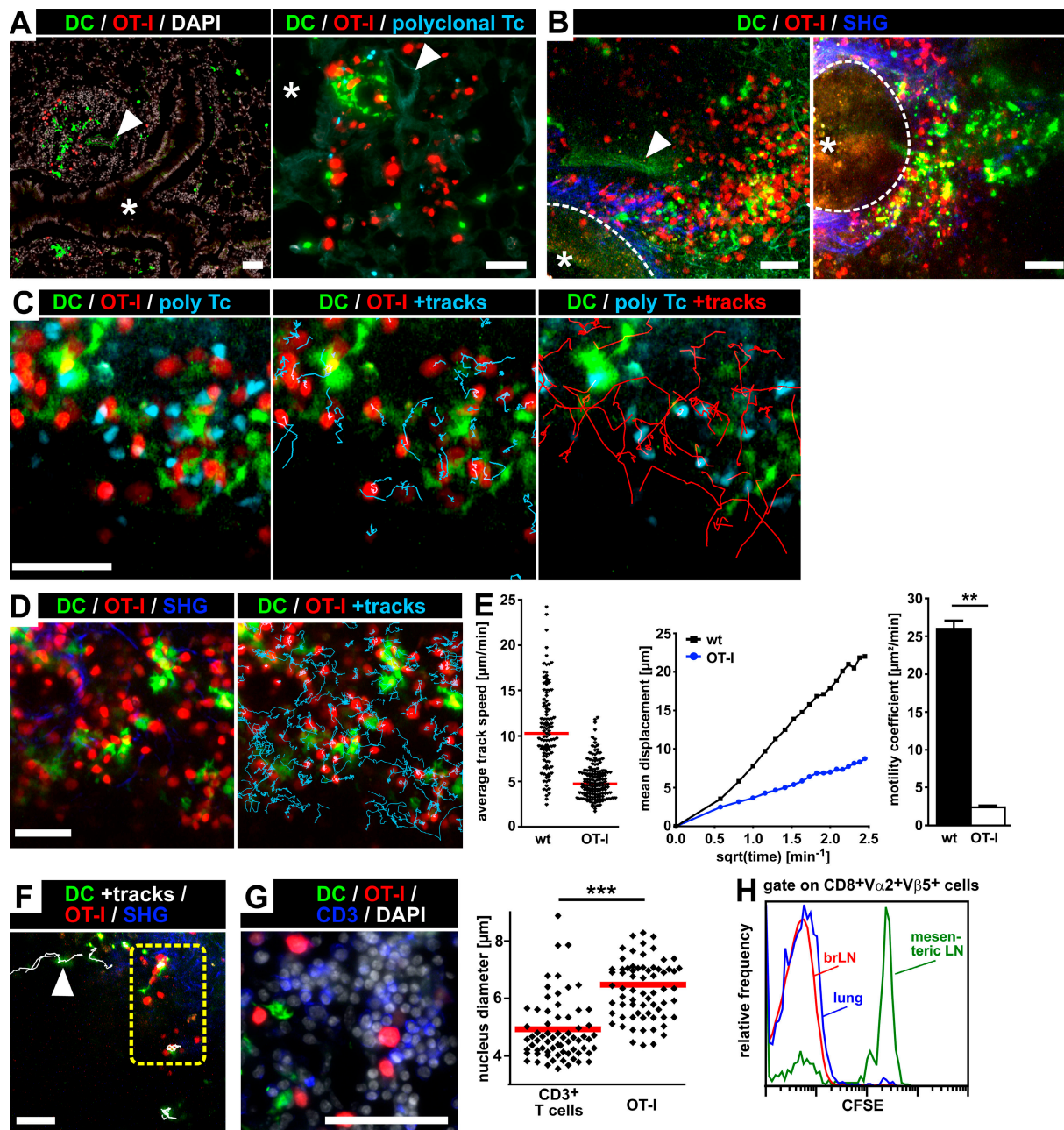
Figure 5. Visualization of antigen–specific T cell–DC interactions during T cell priming within BALT. TAMRA-labeled CD8^{+} OT-I T cells and CMAC-labeled polyclonal CD8^{+} WT T cells were injected i.v. into BALT-bearing recipients. 24 h later, SIINFEKL–loaded EGFP^{+} bone marrow–derived DCs (Ag-DCs) were i.t. transferred into the same animals, and lungs were explanted an additional 24 or 48 h later. (A) Cryosections of paraformaldehyde (PFA)-fixated lungs isolated 24 h after i.t. transfer of Ag-DCs into MVA-treated WT mice. (left) EGFP[+] Ag-DCs and TAMRA^{+} OT-I T cells localize into BALT. (right) Higher magnification image of a BALT structure harboring Ag-DCs, OT-I T cells, and polyclonal CD8^{+} WT T cells. (B) Visualization of BALT within lungs of MVA-treated WT (left) or CCR7^{−/−} (right) mice by ex vivo two-photon microscopy. Maximum intensity projections of three-dimensional imaging volumes (left: eight Z-slices, 7.5-µm spacing; right: seven Z-slices, 6-µm spacing). Collagen fibers surrounding the basal surface of the bronchial epithelium (dashed line) are visualized by SHG. Asterisks represent the bronchial lumen, and arrowheads indicate a blood vessel. (C) Analysis of T cell–DC interactions within BALT of MVA-treated WT mice by two-photon microscopy (excitation wavelength = 780 nm). 24 h after i.t. transfer of EGFP[+] Ag-DCs, TAMRA[+] OT-I T cells exhibit a highly confined migration behavior in the vicinity of Ag-DCs. In contrast, CMAC[+] polyclonal WT control T cells display a much higher motility (Video 1). (D) The experiment was performed as in C but imaged at 865 nm (Video 2). (E) Motility parameter analysis for OT-I and polyclonal CD8^{+} WT T cells migrating within BALT 24 h after transfer of Ag-DCs. (left) Dots represent individual cell tracks, and bars indicate median average track speed. (middle) Mean displacement plots. (right) Motility coefficient (means + SD). **, P < 0.01. (F) 24 h after i.t. transfer of Ag-DCs into CCR7^{−/−} recipients, EGFP[+] DCs were found to enter BALT by directional interstitial migration (arrowhead; Video 3). In contrast, DCs remain largely stationary during Ag presentation within BALT (dashed yellow box; Video 3). Data in A–F are representative of two to four mice per group in two independent experiments.

immunohistological analysis showed that the area of CD11c^{+} pixels per lung section was reduced by >90% 2 d after the second DT treatment (Fig. 4 B), whereas flow cytometry revealed that DCs in mesenteric LNs were not affected by the local application of DT (Fig. 4 C). Of interest, these studies also revealed that BALT was strongly reduced in size in the DT-treated group (Fig. 4 D), whereas the total number of BALT structures per lung was not reduced by DT treatment (not depicted). Collectively, these data indicate that DCs play an essential role in the maintenance of MVA-induced BALT. Because AMs are efficiently depleted by this approach as well (unpublished data), we currently cannot rule out that these cells also contribute to BALT maintenance. However, this hypothesis seems unlikely, as AMs are readily depleted within 1 d after MVA infection (Fig. 2), whereas the DT treatment was not started before day 8 after MVA application.

BALT serves as a general priming site for T cells

The data described so far indicate that the virus-induced formation of BALT participates in generating antivirus immune responses. However, although MVA cannot replicate in mammals and is rapidly cleared from the lung tissue, MVA-induced BALT is maintained for several weeks (Fig. 1 I). We therefore tested the hypothesis that induced BALT might function comparably to a regular lymphoid organ, being able to support the de novo priming of naive T cells bearing TCR specificities that are not related to the BALT–inducing pathogen. To this end, BALT was induced in WT animals by i.n. application of MVA-WT. 18 d later, these mice, as well as untreated CCR7^{−/−} animals, which constitutively develop BALT, received by i.v. injection $2–2.5 \times 10^7$ TAMRA-labeled CD8^{+} OT-I T cells together with $1.5–2 \times 10^7$ CMAC-labeled polyclonal CD8^{+} T cells isolated from C57BL/6 donors. 24 h later, the animals additionally received by intratracheal (i.t.) application LPS-matured EGFP^{+} DCs generated in vitro from the bone marrow of β–actin–EGFP transgenic mice (Okabe et al., 1997) loaded with OVA I peptide (SIINFEKL; Ag-DCs).

Immunohistological analysis of lung cryosections by epifluorescence microscopy (Fig. 5 A) as well as ex vivo two-photon imaging of BALT within 1–2-mm thick lung slices (Fig. 5 B) revealed that adoptively transferred EGFP[+] Ag-DCs as well as TAMRA-labeled OT-I T cells and CMAC-labeled polyclonal T cells were abundantly present in the BALT of MVA-treated WT (Fig. 5, A and B, left) and untreated CCR7^{−/−} (Fig. 5 B, right) recipients. Structural features of BALT, such as adjacent bronchi and blood vessels, were readily identified by their characteristic autofluorescence signals (Fig. 5, A and B), and the second harmonics

generation (SHG) signal resulting from two-photon excitation allowed the additional visualization of collagen fibers surrounding the basal surface of bronchial epithelium (Fig. 5 B). To analyze the cellular dynamics within BALT, lung slices were placed in a custom-built incubation chamber and constantly superfused with oxygenated (95% O_2/5% CO_2) medium at 37°C. Imaging BALT ex vivo 24 and 48 h after the i.t. transfer of Ag-DCs into MVA-treated WT recipients, we found TAMRA-labeled OVA-specific OT-I T cells to interact intensively with EGFP[+] Ag-DCs (Fig. 5, C and D; Videos 1 and 2; and not depicted). Interestingly, the observed migration and interaction behavior of OT-I T cells in BALT was reminiscent of the cellular dynamics reported for CD8^{+} T cells during priming in LNs (Mempel et al., 2004): at 24 h after i.t. DC transfer, long-lasting stable contacts between OT-I T cells and Ag-DCs were predominant, largely confining the migration of interacting OT-I T cells to DC-rich areas of BALT (Fig. 5, C and D; and Videos 1 and 2). At 48 h after i.t. transfer of Ag-DCs, many OT-I T cells were clearly enlarged, exhibiting slow swarming movements in the vicinity of EGFP[+] Ag-DCs (unpublished data), probably indicating the start of their proliferative activity (Mempel et al., 2004). In contrast, CMAC-labeled polyclonal CD8^{+} WT T cells did not engage in stable interactions with Ag-DCs at either time point (Fig. 5 C, Video 1, and not depicted). The quantitative analysis of T cell motility parameters revealed much lower cellular velocities and displacements, and consequently highly reduced motility coefficient values, for OT-I cells when compared with the polyclonal CD8^{+} T cell population (Fig. 5 E and not depicted), further corroborating the antigen-specific nature of the observed OT-I T cell–DC interaction behavior in BALT.

Although we sometimes observed EGFP[+] Ag-DCs to enter BALT by means of a rapid directional interstitial migration during ex vivo imaging (Fig. 5 F and Video 3), it seems likely that DCs can reach BALT via afferent lymphatics as well. Ag-DCs localized to BALT remained largely stationary but exhibited extraordinary probing activity, displaying far-range sweeping dendrite movements during antigen presentation (Fig. 5, D and F; and Videos 2 and 3). We next quantitatively analyzed lung cryosections for the maximum nucleus diameters of TAMRA^{+} OT-I T cells as well as TAMRA^{−}CD3^{+} endogenous T cells present in BALT 48 h after i.t. transfer of Ag-DCs (Fig. 5 G). OT-I T cells displayed significantly larger nuclei compared with resting endogenous T cells, consistent with the idea that the proliferation of antigen-specific T cells activated within BALT had already started at this time point. Finally, we analyzed the proliferation of OT-I T cells by in vivo CFSE dilution at day 4 after the i.t.

(G) TAMRA[+] OT-I T cells within BALT display enlarged cell bodies and nuclei 48 h after i.t. transfer of Ag-DCs. The maximum diameters of DAPI-stained nuclei of TAMRA^{+} (OT-I) as well as TAMRA^{−}CD3^{+} endogenous T cells within BALT were measured on cryosections. Individual values (dots) and means (red bars) of 140 randomly chosen cells from four sections from two mice are shown. ***, P < 0.001. (H) CSFE profiles of OT-I T cells isolated from the lung, brLNs, or mesenteric LNs 4 d after the i.t. transfer of Ag-DCs in mice treated with FTY720 (initial gavage of 1 mg/kg of body weight on day 0, with drinking water supplemented with 2.5 μg/ml FTY720 afterward; representative data of four mice analyzed in two independent experiments). Bars, 50 μm.

transfer of Ag-DCs (Fig. 5 H). The recipient animals were additionally treated with FTY720 to block lymphocyte egress from lymphoid organs. The observation that OT-I T cells isolated from the lungs had proliferated as efficiently as those residing in the brLNs further supports the idea that BALT can indeed function as a local priming site for naive T cells.

Within this study, we demonstrate that a single i.n. application of the replication-deficient vaccine virus MVA, which efficiently infects AMs and DCs, is sufficient to induce long-lasting and highly organized BALT in normal WT mice. DCs in particular seem to represent key organizing cells in BALT biology, as they are among the first cells to be recruited into sites of developing BALT (Fig. 1 B) and depletion of these cells leads to a pronounced regression in BALT size (Fig. 4). Furthermore, antigen-loaded DCs are actively migrating into preexisting BALT where they can present antigen to naive T cells.

Thus, we conclude that induced BALT represents an organized lymphoid structure for antigen presentation by DCs in the lung that is capable of supporting long-lasting T cell–DC interactions as well as the efficient priming of naive T cells. Importantly, the antigenic specificity of the observed priming events (the OVA I peptide SIINFEKL) was completely different from the antigenic nature of the stimulus that had initially induced the formation of BALT (MVA), and occurred long after the complete clearance of the inducing pathogen. Therefore, given its sustained presence, induced BALT can obviously function as a general priming site for T cell responses in the lung.

MATERIALS AND METHODS

Mice. Mice were bred at a local animal facility or purchased from Charles River. CD11c-DOG mice expressing DTR under the control of the CD11c promoter were described previously (Hochweller et al., 2008). B6.129P2(C)-Ccr7^{tm1Rfor}/J mice (CCR7$^{-/-}$) were backcrossed on the C57BL/6 background for >15 generations (Förster et al., 1999). In some experiments, DCs were differentiated from the bone marrow of β-actin–GFP mice (Okabe et al., 1997) using previously described protocols (Ohl et al., 2004). Animal protocols were approved by the institutional review board and the Niedersächsisches Landesamt für Verbraucherschutz und Lebensmittelsicherheit.

MVA. Recombinant MVA constructs have been described previously (Staib et al., 2000; Albrecht et al., 2008). Virus stocks were generated by standard methods (Sutter and Moss, 1992). In brief, viruses were propagated on primary chicken embryo fibroblasts (CEFs), purified by sucrose gradient centrifugation, and titrated on CEFs to determine infectious units. Labeling of MVA with the fluorescent dye Cy5 was performed as described by the manufacturer (GE Healthcare).

i.n. inoculation. Mice were deeply anaesthetized with ketamine/xylazine, and 10^7 IU MVA diluted in 50 μl PBS was applied to the nostrils. For the depletion of CD11c$^+$ cells from the lung, CD11c-DOG mice were i.n. treated with 50 ng DT (Sigma-Aldrich) in 50 μl PBS.

T cell transfer. Blood was taken from CD45.1$^+$ OT-I donors, and 200 CD8$^+$ TCR Vα5$^+$ OT-I cells were injected i.v. into recipients (Fig. 3). For two-photon imaging, CD8$^+$ T cells from OT-I or WT donors were sorted to a purity of 90–95% using a MACS CD8$^+$ T cell isolation kit applying an AutoMACS (Miltenyi Biotec). OT-I T cells were labeled with 15 μM TAMRA, whereas WT T cells were labeled with 15 μM CMAC (both from

Invitrogen). 2–2.5 × 10^7 TAMRA-labeled OT-I T cells and 1.5–2 × 10^7 CMAC-labeled WT T cells were injected i.v. In some experiments, mice additionally received 2 × 10^7 unlabeled OT-I T cells as "competitor" cells.

Organ preparation. BAL fluid was obtained by flushing the lung two times with 1 ml of cold PBS. For lung histology, mice were perfused with 5 ml of ice-cold PBS. The trachea was cut and a 1:1 mixture of Tissue-Tek OCT (Sakura) and PBS was instilled. The lung was removed and snap frozen in OCT. 8-μm sections were performed with a cryostat (CM3050; Leica), as previously described (Hintzen et al., 2006).

Flow cytometry. Single-cell suspensions were prepared by mechanical disruption. Lungs were cut into small pieces and digested with 0.5 mg/ml collagenase D and 0.025 mg/ml DNase I in RPMI 1640 for 30 min at 37°C. Cells were blocked with 5% rat serum, stained, and analyzed with a cytometer (LSRII; BD). Data were analyzed using WinList 6.0 (Verity Software House). The following antibodies were used: CD103-FITC (M290), CD11c-PE (HL3), MHCII-bio (AF6-120.1) detected with streptavidin–Alexa Fluor 750, CD11b-PeCy7 (M1/70), CD11b-PE (M1/70), CD86-allophycocyanin (APC; GL-1), anti-trinitrolphenol–APC (isotype control), CD69PerCp-Cy5.5 (H1.2F3), CD69 (H1.2F3), CD127–Alexa Fluor 488 (A7R34), IFN-γ–PE (XMG1.2), CD3-PE (145-2C11), B220-Cy5 (TIB 146), F4/80-PE (BM8), and CD11c-bio (HL3) detected with streptavidin–Alexa Fluor 488.

Epifluorescence microscopy. Sections were fixed in cold acetone, rehydrated in Tris-buffered saline with 0.05% Tween 20, blocked with 2.5% rat and 2.5% mouse serum, and stained at room temperature for 30 min. Pictures were taken with a fluorescence microscope (Axiovert) using AxioVision 4.6 software (both from Carl Zeiss, Inc.).

BALT area analysis. Overview pictures of lungs were recorded with the mosaic function of the AxioVision software and whole central sections of the lungs were analyzed. The total number of BALT structures was measured as described previously (Kocks et al., 2007). ImageJ (available at http://rsbweb.nih.gov/ij/) was used to determine the percentage of CD11c$^+$ pixel area on pictures taken with identical exposure and display settings.

i.t. DC transfer. EGFP$^+$ bone marrow–derived DCs were generated from the bone marrow of β-actin–EGFP transgenic mice (Okabe et al., 1997) by in vitro culture (Ohl et al., 2004). After overnight LPS maturation and loading with OVA I peptide (SIINFEKL), 2–6 × 10^6 DCs were resuspended in 60 μl PBS and transferred i.t.

Two-photon microscopy. Mice were anesthetized with ketamine/xylazine and bled to death by cutting the vena cava before harvesting the lungs. Horizontal lung slices (thickness = 1–2 mm) were cut with a cryotome blade (Leica), immobilized in an imaging chamber (Fig. S1) using tissue adhesive (Abbott), and superfused with oxygenated (95% O$_2$/5% CO$_2$) RPMI 1640 medium (Invitrogen) containing 1% penicillin/streptomycin, 25 mM Hepes, and 5 g/liter glucose. Imaging was performed on a TriM Scope (LaVision Biotec) equipped with an upright microscope (BX51; Olympus) fitted with a 20× 0.95 NA water immersion objective and a pulsed infrared laser (MaiTai Ti:Sa; Spectra-Physics), tuned to 865 nm for optimal excitation of EGFP and TAMRA and to 780 nm for additional visualization of CMAC. To generate time-lapse series, Z-stacks of up to 10 images were acquired every 20 s.

Data analysis of two-photon imaging was performed as described (Worbs et al., 2007), using Imaris 6.2.1 (Bitplane). Only tracks with durations >60 s were included in the analysis. Average track speed values were calculated using Imaris, whereas mean displacement plots and motility coefficients were calculated using Visual Basic for Applications (Excel; Microsoft).

Statistical analysis. Statistical analysis was performed with Prism 4 (GraphPad Software, Inc.). All significant values were determined using the unpaired two-tailed t test and all error bars represent SDs. Statistical differences for the mean values are as follows: *, $P < 0.05$; **, $P < 0.01$; and ***, $P < 0.001$.

REFERENCES

Albrecht, M., Y. Suezer, C. Staib, G. Sutter, S. Vieths, and G. Reese. 2008. Vaccination with a Modified Vaccinia Virus Ankara-based vaccine protects mice from allergic sensitization. *J. Gene Med.* 10:1324–1333. doi:10.1002/jgm.1256

Bienenstock, J., and D. Befus. 1984. Gut- and bronchus-associated lymphoid tissue. *Am. J. Anat.* 170:437–445. doi:10.1002/aja.1001700316

Corbett, M., W.M. Bogers, J.L. Heeney, S. Gerber, C. Genin, A. Didierlaurent, H. Oostermeijer, R. Dubbes, G. Braskamp, S. Lerondel, et al. 2008. Aerosol immunization with NYVAC and MVA vectored vaccines is safe, simple, and immunogenic. *Proc. Natl. Acad. Sci. USA.* 105:2046–2051. doi:10.1073/pnas.0705191105

Förster, R., A. Schubel, D. Breitfeld, E. Kremmer, I. Renner-Müller, E. Wolf, and M. Lipp. 1999. CCR7 coordinates the primary immune response by establishing functional microenvironments in secondary lymphoid organs. *Cell.* 99:23–33. doi:10.1016/S0092-8674(00)80059-8

Gherardi, M.M., and M. Esteban. 2005. Recombinant poxviruses as mucosal vaccine vectors. *J. Gen. Virol.* 86:2925–2936. doi:10.1099/vir.0.81181-0

Hintzen, G., L. Ohl, M.L. del Rio, J.I. Rodriguez-Barbosa, O. Pabst, J.R. Kocks, J. Krege, S. Hardtke, and R. Förster. 2006. Induction of tolerance to innocuous inhaled antigen relies on a CCR7-dependent dendritic cell–mediated antigen transport to the bronchial lymph node. *J. Immunol.* 177:7346–7354.

Hochweller, K., J. Striegler, G.J. Hämmerling, and N. Garbi. 2008. A novel CD11c.DTR transgenic mouse for depletion of dendritic cells reveals their requirement for homeostatic proliferation of natural killer cells. *Eur. J. Immunol.* 38:2776–2783. doi:10.1002/eji.200838659

Kastenmuller, W., G. Gasteiger, L. Stross, D.H. Busch, and I. Drexler. 2009. Cutting edge: mucosal application of a lyophilized viral vector vaccine confers systemic and protective immunity toward intracellular pathogens. *J. Immunol.* 182:2573–2577. doi:10.4049/jimmunol.0803871

Kocks, J.R., A.C. Davalos-Misslitz, G. Hintzen, L. Ohl, and R. Förster. 2007. Regulatory T cells interfere with the development of bronchus-associated lymphoid tissue. *J. Exp. Med.* 204:723–734. doi:10.1084/jem.20061424

Kocks, J.R., H. Adler, H. Danzer, K. Hoffmann, D. Jonigk, U. Lehmann, and R. Förster. 2009. Chemokine receptor CCR7 contributes to a rapid and efficient clearance of lytic murine gamma-herpes virus 68 from the lung, whereas bronchus-associated lymphoid tissue harbors virus during latency. *J. Immunol.* 182:6861–6869. doi:10.4049/jimmunol.0801826

Kohlmeier, J.E., S.C. Miller, and D.L. Woodland. 2007. Cutting edge: antigen is not required for the activation and maintenance of virus-specific memory CD8+ T cells in the lung airways. *J. Immunol.* 178:4721–4725.

Lehmann, M.H., W. Kastenmuller, J.D. Kandemir, F. Brandt, Y. Suezer, and G. Sutter. 2009. Modified vaccinia virus Ankara triggers chemotaxis of monocytes and early respiratory immigration of leukocytes by induction of CCL2 expression. *J. Virol.* 83:2540–2552. doi:10.1128/JVI.01884-08

Liu, L., R. Chavan, and M.B. Feinberg. 2008. Dendritic cells are preferentially targeted among hematolymphocytes by Modified Vaccinia Virus Ankara and play a key role in the induction of virus-specific T cell responses in vivo. *BMC Immunol.* 9:15. doi:10.1186/1471-2172-9-15

Lührmann, A., T. Tschernig, and R. Pabst. 2002/2003. Stimulation of bronchus-associated lymphoid tissue in rats by repeated inhalation of aerosolized lipopeptide MALP-2. *Pathobiology.* 70:266–269. doi:10.1159/000070740

Mempel, T.R., S.E. Henrickson, and U.H. von Andrian. 2004. T-cell priming by dendritic cells in lymph nodes occurs in three distinct phases. *Nature.* 427:154–159. doi:10.1038/nature02238

Meyer, H., G. Sutter, and A. Mayr. 1991. Mapping of deletions in the genome of the highly attenuated vaccinia virus MVA and their influence on virulence. *J. Gen. Virol.* 72:1031–1038. doi:10.1099/0022-1317-72-5-1031

Moyron-Quiroz, J.E., J. Rangel-Moreno, K. Kusser, L. Hartson, F. Sprague, S. Goodrich, D.L. Woodland, F.E. Lund, and T.D. Randall. 2004. Role of inducible bronchus associated lymphoid tissue (iBALT) in respiratory immunity. *Nat. Med.* 10:927–934. doi:10.1038/nm1091

Ohl, L., M. Mohaupt, N. Czeloth, G. Hintzen, Z. Kiafard, J. Zwirner, T. Blankenstein, G. Henning, and R. Förster. 2004. CCR7 governs skin dendritic cell migration under inflammatory and steady-state conditions. *Immunity.* 21:279–288. doi:10.1016/j.immuni.2004.06.014

Okabe, M., M. Ikawa, K. Kominami, T. Nakanishi, and Y. Nishimune. 1997. "Green mice" as a source of ubiquitous green cells. *FEBS Lett.* 407:313–319. doi:10.1016/S0014-5793(97)00313-X

Ramírez, J.C., M.M. Gherardi, and M. Esteban. 2000. Biology of attenuated modified vaccinia virus Ankara recombinant vector in mice: virus fate and activation of B- and T-cell immune responses in comparison with the Western Reserve strain and advantages as a vaccine. *J. Virol.* 74:923–933. doi:10.1128/JVI.74.2.923-933.2000

Shiow, L.R., D.B. Rosen, N. Brdicková, Y. Xu, J. An, L.L. Lanier, J.G. Cyster, and M. Matloubian. 2006. CD69 acts downstream of interferon-alpha/beta to inhibit S1P1 and lymphocyte egress from lymphoid organs. *Nature.* 440:540–544. doi:10.1038/nature04606

Sminia, T., G.J. van der Brugge-Gamelkoorn, and S.H. Jeurissen. 1989. Structure and function of bronchus-associated lymphoid tissue (BALT). *Crit. Rev. Immunol.* 9:119–150.

Staib, C., I. Drexler, M. Ohlmann, S. Wintersperger, V. Erfle, and G. Sutter. 2000. Transient host range selection for genetic engineering of modified vaccinia virus Ankara. *Biotechniques.* 28:1137–1148.

Sutter, G., and B. Moss. 1992. Nonreplicating vaccinia vector efficiently expresses recombinant genes. *Proc. Natl. Acad. Sci. USA.* 89:10847–10851. doi:10.1073/pnas.89.22.10847

Tschernig, T., and R. Pabst. 2000. Bronchus-associated lymphoid tissue (BALT) is not present in the normal adult lung but in different diseases. *Pathobiology.* 68:1–8. doi:10.1159/000028109

Worbs, T., T.R. Mempel, J. Bölter, U.H. von Andrian, and R. Förster. 2007. CCR7 ligands stimulate the intranodal motility of T lymphocytes in vivo. *J. Exp. Med.* 204:489–495. doi:10.1084/jem.20061706

Xu, B., N. Wagner, L.N. Pham, V. Magno, Z. Shan, E.C. Butcher, and S.A. Michie. 2003. Lymphocyte homing to bronchus-associated lymphoid tissue (BALT) is mediated by L-selectin/PNAd, α4β1 integrin/VCAM-1, and LFA-1 adhesion pathways. *J. Exp. Med.* 197:1255–1267. doi:10.1084/jem.20010685